The effect of intermolecular interaction on excited states in p-DTS(FBTTH$_2$)$_2$

The Journal of Chemical Physics

Markus Reichenberger[1,2], John A. Love[3], Alexander Rudnick[1,2], Sergey Bagnich[1], Fabian Panzer[1,2,4], Anna Stradomska[5], Guillermo C. Bazan[3], Thuc-Quyen Nguyen[3] and Anna Köhler[1,2,*]

[1] Experimental Physics II, University of Bayreuth, 95440 Bayreuth (Germany)

[2] Bayreuth Institute of Macromolecular Research (BIMF), University of Bayreuth, 95440 Bayreuth (Germany)

[3] Center for Polymers and Organic Solids, Departments of Chemistry & Biochemistry and Materials, University of California, Santa Barbara, California 93106 (United States)

[4] Department of Functional Materials, University of Bayreuth, 95440 Bayreuth (Germany)

[5] School of Chemistry, University of Glasgow, Glasgow G12 8QQ (United Kingdom)

[*] Corresponding Author: anna.koehler@uni-bayreuth.de, Phone: +49-921-55-2600, Fax: +49-921-55—2521

Keywords: organic semiconductor, small molecule, phase transition, aggregation, self-assembly, absorption spectroscopy, emission spectroscopy, excited states

Abstract

Using optical spectroscopy in solution and thin film, and supported by quantum chemical calculations, we investigated the aggregation process of the donor-acceptor type molecule p-DTS(FBTTH$_2$)$_2$. We demonstrate that cooling a solution induces a disorder-order phase transition that proceeds in three stages analogous to the steps observed in semi-rigid conjugated polymers. By analyzing the spectra we are able to identify the spectral signature of monomer and aggregate in absorption and emission. From this we find that in films the fraction of aggregates is near 100 % which is in contrast to films made from semi-rigid conjugated polymers.

Introduction

During the last two decades, organic bulk heterojunction (BHJ) solar cells have mostly been made using a conjugated polymer as electron donor and a fullerene derivative as electron acceptor material, as these components are well soluble, blend well and form smooth films with suitable morphologies.[1] In the last few years, highly efficient organic BHJ solar cells have also been prepared that use soluble small molecules as the semiconducting donor component.[2-9] Power conversion efficiencies exceeding 10 % have even been reported when soluble small molecules are used in ternary blends.[10] Soluble small molecules are well-defined in terms of their molecular weight. Compared to conjugated polymers, they can be prepared, characterized and purified easily with a low batch-to-batch variation, which is of advantage for large-scale industrial applications.

A molecular donor that has proven to be particularly suitable for efficient solar cell applications is 7,7'-[4,4-bis(2-ethylhexyl)-4*H*-silolo[3,2-*b*:4,5-*b*']dithiophene-2,6-diyl]bis[6-fluoro-4-(5'-hexyl-[2,2'-bithiophene]-5-yl)benzo[*c*][1,2,5]thiadiazole] (p-DTS(FBTTH$_2$)$_2$) (Figure 1a).[11] The performance of BHJ solar cells made with p-DTS(FBTTH$_2$)$_2$ as donor, however, depends strongly on the film processing conditions. Love et al. demonstrated that different processing methods, such as thermal annealing or using diiodooctane as solvent-additive can strikingly improve the power conversion efficiency of the solar cell.[8] Using electron microscopy and X-ray measurements they could show that the high power conversion efficiencies were associated with an existing network of crystalline grains, where high π-π* overlap ensures good charge transport between adjacent molecules. The π-stacking, however, also manifested itself in the absorption spectra of the BHJ films. In highly efficient solar cells made with a fullerene-derivative as acceptor, the absorption

spectra showed a prominent 0-0 peak of the p-DTS($FBTTH_2$)$_2$, whereas this peak is reduced in less efficient cells. This is also the case when the fullerene is replaced by a perylene diimide (PDI) as acceptor.[12] While electron microscopy and X-ray measurements are expensive and time-consuming techniques, absorption measurements do not require much time and are widely available in laboratories for sample characterization. Moreover, absorption and photoluminescence measurements are also sensitive to short-range order and interactions, which is relevant for the process of exciton dissociation, while many structural techniques are more suitable for long-range order that controls transport properties.

A prerequisite to using optical spectroscopy for sample analysis is that the absorption and emission spectra pertaining to aggregated p-DTS($FBTTH_2$)$_2$ are identified clearly and that they are sufficiently distinct from the spectra of the non-interacting molecules. A clear identification requires in particular a spectral deconvolution of monomer and aggregate spectra. To this end we have investigated the absorption and emission spectra of p-DTS($FBTTH_2$)$_2$ in dilute solution, more concentrated solution and in the thin film as a function of temperature. We identify the spectra pertaining to non-interacting molecules (“monomers”) and those pertaining to ordered, interacting molecules (“aggregates”). The disorder-order transition that we observe upon cooling occurs in three stages, in the same way as for semi-crystalline conjugated polymers. However, owing to the monodispersity of the small molecule sample, the transition is very sharp, in contrast to that observed in polydisperse semi-crystalline polymer samples. Moreover, p-DTS($FBTTH_2$)$_2$ films can be prepared to contain essentially only aggregates, in contrast to thin films made from semi-crystalline polymers that contain typically only up to 60 % of aggregated phase.[13,14]

Experimental Methods

Sample preparation

7,7'-[4,4-bis(2-ethylhexyl)-4*H*-silolo[3,2-*b*:4,5-*b*']dithiophene-2,6-diyl]bis[6-fluoro-4-(5'-hexyl-[2,2'-bithiophene]-5-yl)benzo[*c*][1,2,5]thiadiazole], p-DTS($FBTTH_2$)$_2$, was prepared as reported in ref.[11]. For spectroscopic studies, solutions in 2-methyl-tetrahydrofurane (MTHF) were prepared at two concentrations, that is $4.1 \cdot 10^{-5}$ M ("dilute solution", 0.05 g/l) and $1.6 \cdot 10^{-4}$ M ("more concentrated solution", 0.2 g/l), by stirring overnight at about 50 °C and 500 rpm, to ensure that all of the material was completely dissolved. Solutions for spin-casting thin films were made at a concentration of $6.6 \cdot 10^{-3}$ M (8 g/l). To prepare solutions in ethanol and hexane, both at $1.0 \cdot 10^{-4}$ M (0.12 g/l) and $4.1 \cdot 10^{-5}$ M (0.05 g/l), we first dissolved the p-DTS($FBTTH_2$)$_2$ in a very small amount of MTHF before adding ethanol or hexane. The amount of MTHF was about 1 % of the total final solution. These solutions were always measured immediately after preparation, where all the material seemed to be dissolved and the solution was clear. Over time, e.g. after one hour, solids precipitated out of the ethanol and hexane solution. For measurements, solutions were filled into a 1 mm fused silica cuvette or films were prepared on Spectrosil B quartz substrates by spin-coating out of a 80 °C hot solution at 800 rpm for 60 s.

Absorption and photoluminescence measurements

Absorption and emission spectra for MTHF solutions and films were recorded with a home-built setup in a temperature range between 300 K and 5 K. The samples were placed under helium in a temperature controlled continuous flow helium cryostat from Oxford Instruments. The light source for absorption measurements was a Xenon-

lamp. To achieve minimum light intensity striking the sample, two correlated monochromators were used, one for incident and the other for transmitted light. As detection unit there was a silicon diode connected to a lock-in-amplifier. The emission spectra were corrected for the transmission of the setup.

Photoluminescence measurements were carried out in situ with excitation by a continuous-wave diode laser from Coherent at 405 nm (3.06 eV) and with detection as for the absorption measurements. Absorption and emission spectra were recorded successively at the same temperature and sample spot. The sample cooling was done in steps with a waiting time of 20 minutes after each temperature was reached. The spectra are corrected for changes in absorption or scattering upon lowering the temperature.

Site-selective photoluminescence measurements with the sample in a temperature controlled continuous flow helium cryostat were carried out using the 355 nm pulsed emission from a Nd:YAG laser as input for a computer controlled UV/Vis optical parametric oscillator to obtain a tunable excitation pulse with a duration of 4-5 ns at 10 Hz. The detection system was a charge-coupled device camera from Andor coupled to a MS125 spectrograph.

Absorption and emission spectra in ethanol and hexane solution at room temperature were taken with commercial setups: a Cary 5000 UV/Vis spectrometer from Varian for absorption measurements and a FP-8600 spectral photometer from Jasco for emission measurements.

Quantum chemical calculations

Ground state geometry optimization was performed using density functional theory (DFT), while the vertical excitations and the optimization of the geometry of the first

excited state were performed using time-dependent density functional theory (TD DFT). All calculations were performed with Gaussian09 revision C.01 program.[15] The long-range corrected functional CAM-B3LYP [16] was used, together with 6-31G** basis set, as the previous studies demonstrated that it accurately describes properties of similar molecules.[17-18]

In all calculations the alkyl chains were replaced by methyl groups. No symmetry constraints were imposed on the ground state nor on the excited state geometry. Influence of the solvent (tetrahydrofuran) was modelled using polarizable continuum media model, using the integral equation formalism (IEFPCM). For geometry optimizations, the equilibrium solvation was used, while for the vertical excitations from the ground state a state-specific non-equilibrium solvation was used, where the slow (rotational) component of the solvent response was calculated for the ground state, and only the fast (electronic) contribution was calculated for the excited state.[19-20] The character of the excited states was investigated using natural transition orbitals (NTO).[21]

Results

Figure 1 shows measurements of photoluminescence and absorption of p-DTS($FBTTH_2$)$_2$ in dilute MTHF solution, more concentrated MTHF solution and in the thin film. These spectra serve as a starting point to assess the impact of intermolecular interactions on excited states in p-DTS($FBTTH_2$)$_2$. In dilute solution (Figure 1b), the absorption and emission spectra at room temperature are both broad and show little structure. Upon cooling from 300 K, the absorption spectra slightly shift to lower energies and continuously acquire a more distinct vibrational structure with increasing weight in the 0-0 transition (centred at 2.00 – 1.95 eV in the temperature range 300 – 70 K). In contrast, the emission spectra merely show a minor bathochromic shift and remain broad until 150 K. At lower temperatures, the emission is well structured so that it resembles the mirror image of absorption, and it is shifted further to the blue spectral range. Measurements in steps of about 20 K (see supporting information (SI), Figure S1) indicate that this change in the spectrum occurs discontinuously between 150 K and 130 K.

Quantum chemical calculations show that the ground state geometry of p-DTS($FBTTH_2$)$_2$ is fairly planar, with no torsion between the central dithienosilole (DTS) donor and the fluorobenzothiadiazole acceptor, about 12° of torsion angle between the fluorobenzothiadiazole acceptor and the dithiophene donor, and about 18° of torsion angle between the two thiophenes (Figure 2a). The energy for rotations is in the range of 1 kcal/mol (about 40 meV per molecule),[17] implying that there may be a distribution of angles at room temperature. We therefore attribute the spectral changes in absorption that are observed upon cooling to a gradual freezing out of the rotational dynamics. The relaxed excited state geometry of p-DTS($FBTTH_2$)$_2$ in tetrahydrofurane (THF) is calculated to be entirely flat (Figure 2b). Thus, at least for

lower temperatures such as 210 K and 150 K, where the absorption spectra are already structured, a structured emission with a clear 0-0 transition could be expected. This is in contrast to the broad emission that is observed. A well-structured emission spectrum is, however, observed even at room temperature when p-DTS($FBTTH_2$)$_2$ is dissolved in the non-polar solvent hexane. This is shown as dotted line in Figure 1b. An analysis of the natural transition orbitals of p-DTS($FBTTH_2$)$_2$ indicates that the first excited state has some charge-transfer character, with the electron density being transferred from the central and outer donor units, DTS and dithiophene, to the fluorobenzothiadiazole acceptor (Figure 2c). Associated with this charge transfer is the increase in dipole moment. The dipole moment for the molecule in THF is calculated to be 0.64 D in the ground state. Upon vertical excitation, a dipole moment of 1.77 D is calculated which reduces slightly to 1.33 D in the relaxed excited state geometry in THF. Evidently, the bathochromic shift and the lack of vibrational structure in the emission spectra taken in the moderately polar solvent MTHF – in contrast to the non-polar solvent hexane – can be attributed to interaction between the excited p-DTS($FBTTH_2$)$_2$ and the polar solvent. Upon excitation of p-DTS($FBTTH_2$)$_2$, the MTHF molecules rearrange their position and orientation to optimize their electrostatic interaction with the solute, such as to minimize the overall energy. The broadening arises from a distribution of polarization energies since the positions and orientations of the solvent molecules fluctuate in the liquid phase. Below the glass transition temperature of MTHF, which is at 137 K, a rearrangement of solvent molecules is no longer possible. As a result, the emission energy is only lowered due to the electronic polarization of the MTHF molecules, while the structure is retained.

When a four times more concentrated MTHF solution is investigated (Figure 1d), no differences arise compared to the dilute solution for temperatures down to 205 K. At lower temperatures, an additional absorption peak arises centered at about 1.8 eV. While the onset of emission at 150 K still occurs at the same energy as for the dilute solution, i.e. at about 1.9 eV, the peak of emission shifts to lower energies and an additional shoulder near 1.4 eV emerges. The spectrum is better resolved at 70 K, so that three features are clearly discernible at about 1.42 eV, 1.65 eV and 1.85 eV. At 70 K, the striking observation of an emission peak (at 1.85 eV) at higher energy than the lowest-energy absorption peak (at 1.80 eV) of the same material gives an indication that two different species may be giving rise to these spectra.

It is noteworthy that the absorption and emission spectra measured in concentrated solution are still distinct from thin film room temperature spectra (Figure 1c). The position of the lowest-energy absorption peak at about 1.80 eV matches that of the more concentrated solution, yet the weight in the vibrational peaks differs. The emission is broad and unstructured with a center energy of 1.55 eV.

The additional contribution to the spectra, which emerges in the more concentrated solution, can be identified by subtracting the spectra taken at the same temperature yet at two different concentrations from each other. This is displayed in Figure 3. To allow for the subtraction, the low-concentration spectrum needs to be normalized in overall intensity such as to match the high energy part of the spectrum. It is also necessary to shift the low-concentration spectrum by 40 meV to the blue spectral range in order to account for the concentration-dependent solvent-shift of on the transition energy.[22] Very similar spectra result when using alternative approaches to separate the two contributions, i.e. by subtracting the spectrum just above the

transition temperature from the spectrum just below the transition temperature, with both spectra having the same concentration, or by modelling the spectrum as a sum of two Franck-Condon progressions. These approaches are detailed in the SI (Figures S2 and S3).

We attribute the additional absorption and emission in the more concentrated solution to interacting p-DTS(FBTTH$_2$)$_2$ such as dimers or larger aggregates. The relative amount of monomers and aggregates can be deduced from the spectra when the change in oscillator strength ε upon aggregation is taken into account.[23] For this, we compare the absorption spectrum at 205 K containing only monomer absorption with the absorption spectrum at 198 K that contains monomer absorption and aggregate absorption. The spectra and the deconvolution in monomer and aggregate absorption are shown in the supporting information, Figure S4. Upon lowering the temperature from 205 K to 198 K, the absorption from the aggregates appears. Upon aggregation, the monomer absorption reduces by $\int \Delta I_M(\lambda) d\lambda$, where $\Delta \mathrm{I_M}$ is the difference in the monomeric absorption prevailing at 205 K and 198 K. At the same time, an aggregate absorption of $\int \Delta I_A(\lambda) d\lambda$ appears. Here, ΔI_A is the aggregate absorption prevailing at 198 K. Since the absorption by the monomer (aggregate) is proportional to the oscillator strength of the monomer, ε_M, (of the aggregate, ε_A), it follows that the ratio F between the oscillator strength of the two species can therefore be deduced by

$$F = \frac{\int \Delta I_A(\lambda) d\lambda}{\int \Delta I_M(\lambda) d\lambda} = \frac{\varepsilon_A}{\varepsilon_M}.$$

As detailed by Clark et al. in Ref. [23] and in the associated supporting information, this approach is only valid when an isosbestic point is formed upon the transition, which is the case here (see Figures S11 in the supplementary information). We find

that the area ratio F from the aggregate-induced absorption compared to the reduction in monomeric absorption is $F = 0.64$. Thus, the oscillator strength in the aggregates is only about two thirds of that in the monomer. Using this result, we derive a maximum fraction of about 0.45 of aggregates in the more concentrated solution. The evolution of the fraction of aggregates with temperature, shown in Figure 3d, shows a very steep onset at 200 K, and an only shallow evolution below 150 K.

The appearance of aggregation upon cooling a solution has been reported before for some π-conjugated polymers, such as P3HT, MEH-PPV and PCPDTBT.[13-14, 24-26] For these polymers, the process of aggregation upon cooling was found to proceed in three distinct phases, i.e. (i) a swelling up and planarization upon cooling, (ii) a transition with an isosbestic point, and (iii) a further planarization of the aggregates formed. The detailed display of the temperature-dependent absorption spectra in Figure 4b indicates that even though p-DTS(FBTTH$_2$)$_2$ is *not* a polymer, aggregation seems to take place in the same fashion. Of course, the red-shift of absorption in the range from 300 K to 205 K does not indicate a swelling up of the molecular structure but rather an increasing conjugation and planarity due to a reduction in torsional dynamics, as mentioned above. Yet, the isosbestic point in the transition range (204 K to 170 K) and the ongoing planarization at lower temperatures are evident in the absorption spectra in the same manner as for the polymers mentioned above.

The evolution of the emission spectra (Figure 4a), in contrast, is more unusual. In the range from 300 K to 205 K, the photoluminescence intensity reduces in contrast to the absorption. In the range from 204 K to 170 K, where aggregate absorption appears, the photoluminescence intensity reduces further. The overall

emission increases, however, from 150 K on to lower temperatures. The reduction in photoluminescence intensity upon cooling in the temperature range above 150 K also occurs for the more dilute solution, yet to a weaker degree. It is accompanied by a concomitant reduction in photoluminescence lifetime (see Figures S5, S6). The origin for this additional decay channel above 150 K is not clear. We speculate that upon cooling, some colliding molecules may form excimer-type states that are non-emissive. Such a phenomenon has been observed previously for pyrene-derivatives in the concentration range preceding the formation of aggregates.[27] For the more concentrated solution in the 204 K - 170 K range, some reduction in photoluminescence intensity can be attributed to the reduced oscillator strength of the aggregates that has been shown to be 64 % of the monomer oscillator strength by the analysis of the absorption spectra. The strong increase in photoluminescence intensity below 150 K at roughly constant absorption strength suggests a freezing out of a non-radiative decay channel. Beside the more special case of possible excimer formation, a significant and typical non-radiative decay mechanism in organic molecules is intersystem crossing from the excited singlet to the triplet state. In the absence of heavy metals, the necessary spin-orbit coupling for this is usually provided by vibrations that mix σ- and π-orbitals, such as ring rotations.[28] In the glassy matrix that prevails below 150 K, both translational and rotational motions are impeded, so that not only excimer formation but, moreover, intersystem crossing should be suppressed.[22] We attribute the increase in photoluminescence intensity below 150 K to this mechanism, in particular for the higher energy emission that is due to the planarized monomer.

Site-selective photoluminescence spectroscopy has been employed to further confirm that the spectra of the higher concentrated solution are composed of two

contributions. Figure 5a displays the photoluminescence spectra obtained for excitation at different energies. For ease of reference, these energies are indicated by arrows in the associated absorption spectra shown in Figure 5b. Nearly identical emission spectra result when the more concentrated MTHF solution is excited at different energies between 1.82 eV and 3.06 eV at room temperature. This clearly confirms the absence of any aggregate emission at 295 K. The absorption at 60 K has, in the context of Figure 3, been attributed to a monomeric and an aggregate contribution. When exciting at a position where only the aggregate absorbs, i.e. at 1.82 eV, the emission features only two clear peaks at about 1.45 eV and 1.60 eV, in good agreement with the peak positions derived from the difference between the emission spectra of more and less dilute solution (see Figure 3). These two features also remain clearly visible when exciting at the onset of the second absorption band, at 2.81 eV and at 3.06 eV, which was the excitation energy used throughout this study. In addition, peaks at 1.85 eV and 1.70 eV superimpose, which matches the position of the photoluminescence peaks observed at 70 K in the more dilute solution (see Figure 1). The latter two peaks dominate the spectrum when exciting at 2.21 eV, i.e. in the center of the monomer absorption. Thus, the site-selective emission spectra confirm the spectral deconvolution presented in Figure 3.

A $1.0 \cdot 10^{-4}$ M solution of the very polar solvent ethanol was investigated at room temperature, in order to obtain insight into the spectra resulting from only aggregates (Figure 5a, bottom panel and Figure 5b, dotted line). We repeated the measurements using a $4.1 \cdot 10^{-5}$ M solution and obtained identical absorption and emission spectra. In a $4.1 \cdot 10^{-5}$ M solution, energy transfer from individual molecules dissolved in solution to aggregates can be excluded. Thus, the lack of monomeric emission, i.e. emission above 1.8 eV in Figure 5a, bottom panel, for excitation at

2.81 eV or 2.21 eV testifies on the absence of monomers. This implies that the associated absorption spectrum can be attributed to absorption from aggregates. This aggregate absorption spectrum in Figure 5b is in good agreement with the spectrum derived by spectral deconvolution (c.f. Figure 3b). The emission obtained for excitation at 1.82 eV matches the spectral range where aggregate emission is observed, though the spectral shape differs.

The difference in spectral shape seen in MTHF, ethanol and film requires clarification. Figure 6 compares the room temperature absorption and emission spectra. From the nearly identical absorption spectra obtained in ethanol and in the thin film we can conclude that a film spun from MTHF solution contains merely aggregated regions without any significant amount of amorphous regions. Recall that we use the term “aggregate” to denote electronically interacting molecules with at least short-range order, as opposed to molecules in an amorphous environment that interact merely by van der Waals forces.

In absorption, the spectra obtained in ethanol or thin film differ from those obtained in MTHF by a bathochromic shift of about 200 meV and by being more structured. The peak positions and intensities in ethanol/thin film are consistent with those observed for the aggregates in MTHF solution (see Figure 3 and Figures S2 and S3 in the supporting information), so that the spectra obtained in ethanol/thin film can be attributed to the aggregates. The additional observation of vibrational structure in the aggregate absorption suggests a more pronounced contribution of $\pi\pi^*$ transitions compared to the dominant charge-transfer character of the non-aggregated species.

In emission, the difference between the aggregate emission in ethanol or in the thin film on the one hand and in low-temperature MTHF solution on the other

hand is more striking. While the spectral position of the room temperature emission in ethanol/thin film agrees with that observed for the aggregate emission in MTHF as shown in Figure 3, the spectral shape differs. A better resolution can be obtained when considering the thin film photoluminescence spectra at low temperature. Upon cooling, the line width reduces and both, absorption and emission shift to lower energy by about 40-60 meV. As a result of the smaller line width, two clear peaks emerge at 1.48 eV and 1.63 eV in the 50 K emission spectra. These peak positions are identical to those observed for the aggregates in MTHF solution (see Figure 3), yet the relative weight between the 0-0 and the 0-1 peak differs.

On the basis of quantum chemical calculations, Spano suggested the relative intensity of the 0-0 peak in aggregate emission to depend on the degree of energetic disorder that is present in the sample.[29] Thus, it appears that there is a higher degree of order in the aggregates formed in ethanol or thin film than in frozen MTHF. This is plausible considering that only aggregates prevail in ethanol/thin film, whereas aggregated and monomeric species are present in almost equal ratios in frozen MTHF as shown above. We therefore attribute the difference in relative 0-0 peak intensity between the emission spectra in MTHF on the one hand and ethanol or film on the other hand to differences in the local environment in which the aggregates are embedded, which affects energetic disorder and excited state correlation.[29]

Discussion

There are two aspects of this study that are of important value. First, the clear identification of the absorption and emission spectra from aggregated p-DTS($FBTTH_2$)$_2$ allows for quick routine evaluation of films intended for solar cells and the processing techniques applied.

Second, p-DTS($FBTTH_2$)$_2$ is a low molecular weight compound with a polydispersity of unity. It is enlightening to compare the process of aggregation in this semi-rigid molecule to that observed in semi-rigid polymers. In the same ways as in polymers, we observe that aggregation proceeds in a three-step process, where the actual process of dimer/aggregate formation is preceded by planarization of the molecular backbone, and followed by further optimization of the aggregate geometry.[13, 24] It appears that the process of planarization is required *a priori* to enable the intermolecular interaction.

For polymers, this is not an obvious requirement since excited state delocalisation along a planarized chain reduces the strength of excitonic coupling between chains.[30-34] Nevertheless, pre-aggregation planarization is unambiguously observed for example for the polymers MEH-PPV, P3HT and PCPDTBT.[13-14, 24-26, 35] It has been predicted in Monte-Carlo simulations for semi-rigid polymers [36] and was also observed in molecular dynamic calculations for MEH-PPV [28]. In a naïve picture, it may be tempting to invoke steric requirements for the aggregation of polymer chains.

The pre-aggregation planarization evidenced in *p*-DTS($FBTTH_2$)$_2$ by the red-shift in absorption and emission spectra (Figure 4) is consistent with temperature-dependent absorption measurement on poly(*p*-phenylene vinylene) oligomers. There,

the occurrence of aggregation in solution correlates with the nature of the side chain. In oligomers with alkoxy side chains, ground and excited states are planar and aggregation in MTHF solution is observed. In contrast when the oligomer carries alkyl side chains, aggregation in MTHF solution cannot be induced by reducing temperature, and this is associated with a twisted ground state geometry and a non-planar excited state geometry.[37] The ground state geometry of p-DTS(FBTTH$_2$)$_2$ in MTHF is fairly flat (see Figure 2), with planar central units and torsion angles of only 12° and 18° to the outer two thiophene rings. After aggregation, e.g. in a single crystal structure, an entirely planar conformation is observed by X-ray studies.[8] In view of the weak torsions in the ground state conformation in MTHF, it is remarkable that planarization necessarily *precedes* aggregation and is not simply induced as geometric reorganization after aggregation. Arguments based on steric requirements that one may invoke for polymers are certainly not convincing in the case of this molecule. A more compelling explanation is that an increasing planarization, resulting from the freezing out of torsional dynamics, reduces the solubility of the molecule in the solvent, so that a reduced solvation dynamics assists the formation of aggregates.[28, 35]

A further illuminating aspect in this comparison of the disorder-order transition between π-conjugated polymers and molecules consists in the remarkable sharpness of the transition observed in Figure 3d. For commercial MEH-PPV or P3HT samples with polydispersity indices (PDIs) exceeding 2, the disorder-order transition is smeared out over a large temperature range, so that their temperature dependence resembles a second order phase transition.[13, 25] In contrast, well-defined P3HT polymer samples with different molecular weights, yet low polydispersity index of PDI < 1.2, have a more narrow transition range that results in a steeper

appearance of the transition. The transition temperature itself, defined as the point of inflexion when the fraction of aggregates is displayed versus temperature, reduces with molecular weight, in agreement with the theoretical description of Sanchez et al. for a disorder-order transition.[38] It was suggested that the broadness of the transition observed for polydisperse polymer samples may result from a superposition of different transition temperatures for the different molecular weight fractions contained in the polydisperse sample.[13] The extremely narrow transition range observed for the monodisperse p-DTS($FBTTH_2$)$_2$ clearly confirms our earlier studies and testifies to the first order nature of this transition. The width of the transition can be quantified by considering the Full Width at Half Maximum (FWHM) of the first derivative to the temperature dependence of the aggregate fraction, as shown in Figure S7 (SI). By this measure, the p-DTS($FBTTH_2$)$_2$ sample with a PDI = 1 has a FWHM of 6 K, P3HT with PDI = 1.2 has a FWHM of 14 K and commercial P3HT with PDI = 2 has a FWHM of 35 K. Both P3HT have a comparable molecular weight of 19±1 kD.

In summary, the spectroscopic investigation of aggregation in p-DTS($FBTTH_2$)$_2$ in dilute solution, more concentrated solution and in the thin film has allowed us to identify the aggregate signature. With this tool, the absorption spectra of solar cells comprising p-DTS($FBTTH_2$)$_2$ can be analysed to infer the fraction of aggregates in the solar cell without need for expensive and time-consuming structural techniques. The latter will only be required when information on long-range order is desired. Moreover, the comparison of the aggregate formation in this stiff molecule to that in π-conjugated polymers has highlighted the importance of torsional dynamics in the aggregation process.

Acknowledgements

We gratefully acknowledge support from the Hanns-Seidel-Stiftung through a stipend to MR by funds from the German Federal Ministry of Education and Research (BMBF), support from the German Science Foundation through the Research Training Group GRK 1640 “Photophysics of Synthetic and Biological Multichromophoric Systems“ and from the State of Bavaria through the Research Network “Solar Technologies go Hybrid”. J.A.L, G.C.B, and T.-Q.N thank the Department of the Navy, Office of Naval Research (Award No. N00014-14-1-0580) for the support. T.-Q.N thanks the Camille Dreyfus Teacher Scholar Award.

Supporting Information:

See supplemental material at [URL will be inserted by AIP] for the following:

Figures S1 to S7 contain the photoluminescence and absorption spectra taken in $4.1 \cdot 10^{-5}$ M MTHF solution at different temperatures; Spectral separation of photoluminescence and absorption in a $1.6 \cdot 10^{-4}$ M MTHF solution at different temperatures into a spectral contribution attributed to monomer and to aggregates; Franck Condon fits to the photoluminescence and absorption spectra of monomer and aggregates; The Raman spectrum; Comparison of the absorption in $1.6 \cdot 10^{-4}$ M MTHF solution at 205 K and at 198 K; Photoluminescence and absorption spectra in a $4.1 \cdot 10^{-5}$ M MTHF solution at different temperatures; The fluorescence decay curves in a $4.1 \cdot 10^{-5}$ M MTHF solution at different temperatures; The first derivative of the fraction of aggregates plotted against relative temperature.

For ease of reference, Figures S8 to S11 give absorption and photoluminescence spectra in a $1.6 \cdot 10^{-4}$ M MTHF solution at different temperatures, measured in fine temperature steps and over a broad energy range; Photoluminescence and absorption spectra in $4.1 \cdot 10^{-4}$ M MTHF solution at different temperatures; Photoluminescence spectra in a thin film at different temperatures; Absorption spectra in $1.6 \cdot 10^{-4}$ M MTHF solution at temperatures between 205 K and 150 K forming an isosbestic point at 1.94 eV.

References

1. Thompson, B. C.; Frechet, J. M. Polymer-fullerene composite solar cells. *Angew. Chem., Int. Ed. Engl.* **2008**, *47*, 58-77.

2. Walker, B.; Kim, C.; Nguyen, T.-Q. Small Molecule Solution-Processed Bulk Heterojunction Solar Cells†. *Chem. Mater.* **2011**, *23*, 470-482.

3. Sun, Y.; Welch, G. C.; Leong, W. L.; Takacs, C. J.; Bazan, G. C.; Heeger, A. J. Solution-processed small-molecule solar cells with 6.7% efficiency. *Nat. Mater.* **2012**, *11*, 44-48.

4. Lin, Y.; Li, Y.; Zhan, X. Small molecule semiconductors for high-efficiency organic photovoltaics. *Chem. Soc. Rev.* **2012**, *41*, 4245-4272.

5. Mishra, A.; Bauerle, P. Small molecule organic semiconductors on the move: promises for future solar energy technology. *Angew. Chem., Int. Ed. Engl.* **2012**, *51*, 2020-2067.

6. Huang, Y.; Kramer, E. J.; Heeger, A. J.; Bazan, G. C. Bulk heterojunction solar cells: morphology and performance relationships. *Chem. Rev.* **2014**, *114*, 7006-7043.

7. Takacs, C. J.; Sun, Y.; Welch, G. C.; Perez, L. A.; Liu, X.; Wen, W.; Bazan, G. C.; Heeger, A. J. Solar cell efficiency, self-assembly, and dipole-dipole interactions of isomorphic narrow-band-gap molecules. *J. Am. Chem. Soc.* **2012**, *134*, 16597-16606.

8. Love, J. A.; Proctor, C. M.; Liu, J.; Takacs, C. J.; Sharenko, A.; van der Poll, T. S.; Heeger, A. J.; Bazan, G. C.; Nguyen, T.-Q. Film Morphology of High Efficiency Solution-Processed Small-Molecule Solar Cells. *Adv. Funct. Mater.* **2013**, *23*, 5019-5026.

9. Love, J. A.; Nagao, I.; Huang, Y.; Kuik, M.; Gupta, V.; Takacs, C. J.; Coughlin, J. E.; Qi, L.; van der Poll, T. S.; Kramer, E. J., et al. Silaindacenodithiophene-based molecular donor: morphological features and use in the fabrication of compositionally tolerant, high-efficiency bulk heterojunction solar cells. *J. Am. Chem. Soc.* **2014**, *136*, 3597-3606.

10. Zhang, J.; Zhang, Y.; Fang, J.; Lu, K.; Wang, Z.; Ma, W.; Wei, Z. Conjugated Polymer-Small Molecule Alloy Leads to High Efficient Ternary Organic Solar Cells. *J. Am. Chem. Soc.* **2015**, *137*, 8176-8183.

11. van der Poll, T. S.; Love, J. A.; Nguyen, T. Q.; Bazan, G. C. Non-basic high-performance molecules for solution-processed organic solar cells. *Adv. Mater.* **2012**, *24*, 3646-3649.

12. Sharenko, A.; Gehrig, D.; Laquai, F.; Nguyen, T.-Q. The Effect of Solvent Additive on the Charge Generation and Photovoltaic Performance of a Solution-Processed Small Molecule:Perylene Diimide Bulk Heterojunction Solar Cell. *Chem. Mater.* **2014**, *26*, 4109-4118.

13. Panzer, F.; Bässler, H.; Lohwasser, R.; Thelakkat, M.; Köhler, A. The Impact of Polydispersity and Molecular Weight on the Order-Disorder Transition in Poly(3-hexylthiophene). *J. Phys. Chem. Lett.* **2014**, *5*, 2742-2747.

14. Scharsich, C.; Fischer, F. S. U.; Wilma, K.; Hildner, R.; Ludwigs, S.; Köhler, A. Revealing structure formation in PCPDTBT by optical spectroscopy. *J. Polym. Sci., Part B: Polym. Phys.* **2015**, *53*, 1416-1430.

15. Frisch, M. J.; Trucks, G. W.; Schlegel, H. B.; Scuseria, G. E.; Robb, M. A.; Cheeseman, J. R.; Scalmani, G.; Barone, V.; Mennucci, B.; Petersson, G. A., et al. *Gaussian 09, Revision C.01*, Gaussian, Inc.: Wallingford, CT, USA, **2009**.

16. Yanai, T.; Tew, D. P.; Handy, N. C. A new hybrid exchange-correlation functional using the Coulomb-attenuating method (CAM-B3LYP). *Chem. Phys. Lett.* **2004**, *393*, 51-57.

17. Coughlin, J. E.; Zhugayevych, A.; Bakus, R. C.; van der Poll, T. S.; Welch, G. C.; Teat, S. J.; Bazan, G. C.; Tretiak, S. A Combined Experimental and Theoretical Study of Conformational Preferences of Molecular Semiconductors. *J. Phys. Chem. C* **2014**, *118*, 15610-15623.

18. Zhugayevych, A.; Postupna, O.; Bakus, R. C.; Welch, G. C.; Bazan, G. C.; Tretiak, S. Ab Initio Study of a Molecular Crystal for Photovoltaics: Light Absorption, Exciton and Charge Carrier Transport. *J. Phys. Chem. C* **2013**, *117*, 4920-4930.

19. Improta, R.; Barone, V.; Scalmani, G.; Frisch, M. J. A state-specific polarizable continuum model time dependent density functional theory method for excited state calculations in solution. *J. Chem. Phys.* **2006**, *125*, 054103.

20. Improta, R.; Scalmani, G.; Frisch, M. J.; Barone, V. Toward effective and reliable fluorescence energies in solution by a new state specific polarizable continuum model time dependent density functional theory approach. *J. Chem. Phys.* **2007**, *127*, 074504.

21. Martin, R. L. Natural transition orbitals. *J. Chem. Phys.* **2003**, *118*, 4775-4777.

22. Köhler, A.; Bässler, H. Electronic Processes in Organic Semiconductors: An Introduction. *Wiley-VCH, Weinheim, ISBN 978-3-527-33292-2,* **2015**.

23. Clark, J.; Chang, J.-F.; Spano, F. C.; Friend, R. H.; Silva, C. Determining exciton bandwidth and film microstructure in polythiophene films using linear absorption spectroscopy. *Appl. Phys. Lett.* **2009**, *94*, 163306.

24. Panzer, F.; Sommer, M.; Bässler, H.; Thelakkat, M.; Köhler, A. Spectroscopic Signature of Two Distinct H-Aggregate Species in Poly(3-hexylthiophene). *Macromolecules* **2015**, *48*, 1543-1553.

25. Köhler, A.; Hoffmann, S. T.; Bässler, H. An order-disorder transition in the conjugated polymer MEH-PPV. *J. Am. Chem. Soc.* **2012**, *134*, 11594-11601.

26. Unger, T.; Panzer, F.; Consani, C.; Koch, F.; Brixner, T.; Bässler, H.; Köhler, A. Ultrafast Energy Transfer between Disordered and Highly Planarized Chains of Poly[2-methoxy-5-(2-ethylhexyloxy)-1,4-phenylenevinylene] (MEH-PPV). *ACS Macro Lett.* **2015**, *4*, 412-416.

27. Haedler, A. T.; Misslitz, H.; Buehlmeyer, C.; Albuquerque, R. Q.; Köhler, A.; Schmidt, H. W. Controlling the pi-stacking behavior of pyrene derivatives: influence of H-bonding and steric effects in different states of aggregation. *Chem. Phys. Chem.* **2013**, *14*, 1818-1829.

28. De Leener, C.; Hennebicq, E.; Sancho-Garcia, J. C.; Beljonne, D. Modeling the dynamics of chromophores in conjugated polymers: the case of poly(2-methoxy-5-(2'-ethylhexyl)oxy 1,4-phenylene vinylene) (MEH-PPV). *J. Phys. Chem. B* **2009**, *113*, 1311-1322.

29. Spano, F. C.; Silva, C. H- and J-aggregate behavior in polymeric semiconductors. *Annu. Rev. Phys. Chem.* **2014**, *65*, 477-500.

30. Barford, W. Exciton transfer integrals between polymer chains. *J. Chem. Phys.* **2007**, *126*, 134905.

31. Clark, J.; Silva, C.; Friend, R. H.; Spano, F. C. Role of Intermolecular Coupling in the Photophysics of Disordered Organic Semiconductors: Aggregate Emission in Regioregular Polythiophene. *Phys. Rev. Lett.* **2007**, *98*, 206406.

32. Cornil, J.; dos Santos, D. A.; Crispin, X.; Silbey, R.; Brédas, J. L. Influence of Interchain Interactions on the Absorption and Luminescence of Conjugated Oligomers and Polymers: A Quantum-Chemical Characterization. *J. Am. Chem. Soc.* **1998**, *120*, 1289-1299.

33. Gierschner, J.; Huang, Y. S.; Van Averbeke, B.; Cornil, J.; Friend, R. H.; Beljonne, D. Excitonic versus electronic couplings in molecular assemblies: The importance of non-nearest neighbor interactions. *J. Chem. Phys.* **2009**, *130*, 044105.

34. Scharsich, C.; Lohwasser, R. H.; Sommer, M.; Asawapirom, U.; Scherf, U.; Thelakkat, M.; Neher, D.; Köhler, A. Control of aggregate formation in poly(3-hexylthiophene) by solvent, molecular weight, and synthetic method. *J. Polym. Sci., Part B: Polym. Phys.* **2012**, *50*, 442-453.

35. Chang, M.; Lee, J.; Kleinhenz, N.; Fu, B.; Reichmanis, E. Photoinduced Anisotropic Supramolecular Assembly and Enhanced Charge Transport of Poly(3-hexylthiophene) Thin Films. *Adv. Funct. Mater.* **2014**, *24*, 4457-4465.

36. Kolinski, A.; Skolnick, J.; Yaris, R. The Collapse Transition of Semiflexible Polymers - a Monte-Carlo Simulation of a Model System. *J. Chem. Phys.* **1986**, *85*, 3585-3597.

37. Hoffmann, S. T.; Bässler, H.; Köhler, A. What determines inhomogeneous broadening of electronic transitions in conjugated polymers? *J. Phys. Chem. B* **2010**, *114*, 17037-17048.

38. Sanchez, I. C. Phase Transition Behavior of the Isolated Polymer Chain. *Macromolecules* **1979**, *12*, 980-988.

Figures and Figure captions

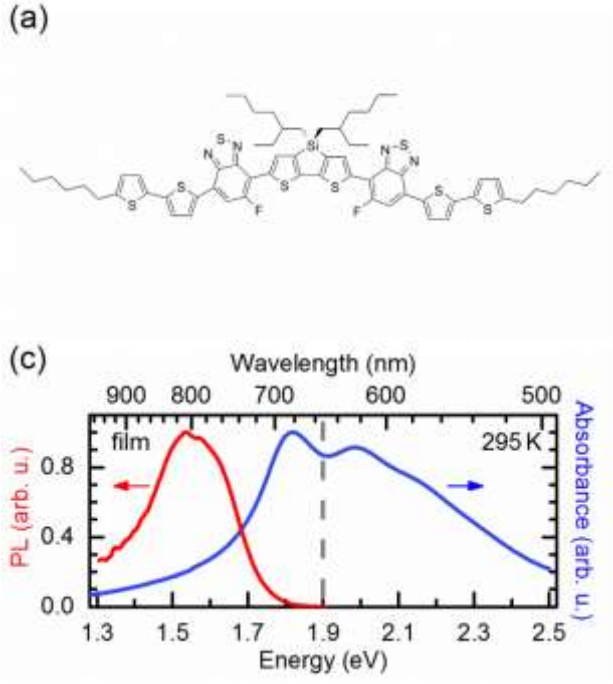

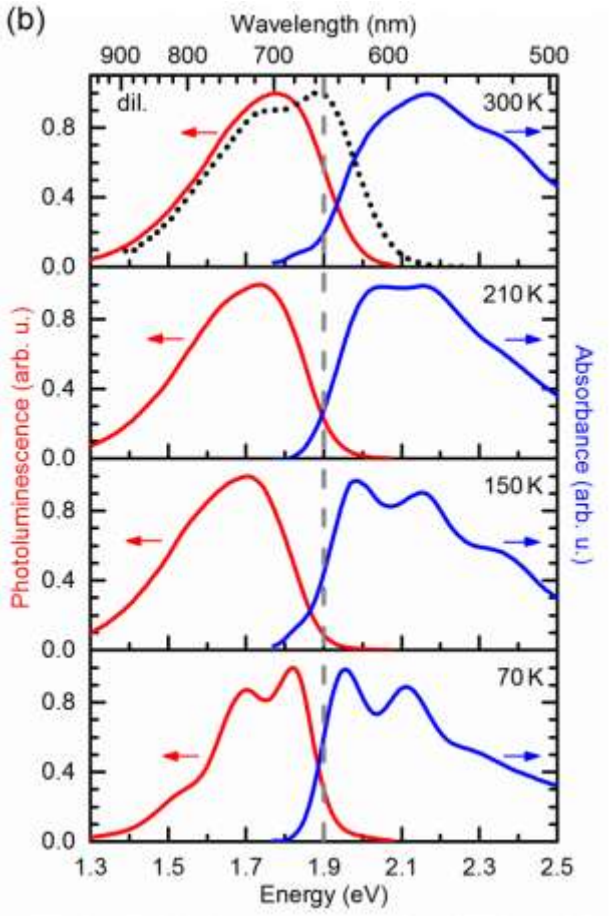
(b)
Wavelength (nm)
900 800 700 600 500
dil.
300 K
210 K
150 K
70 K
Photoluminescence (arb. u.)
Absorbance (arb. u.)
0.0 0.4 0.8
1.3 1.5 1.7 1.9 2.1 2.3 2.5
Energy (eV)

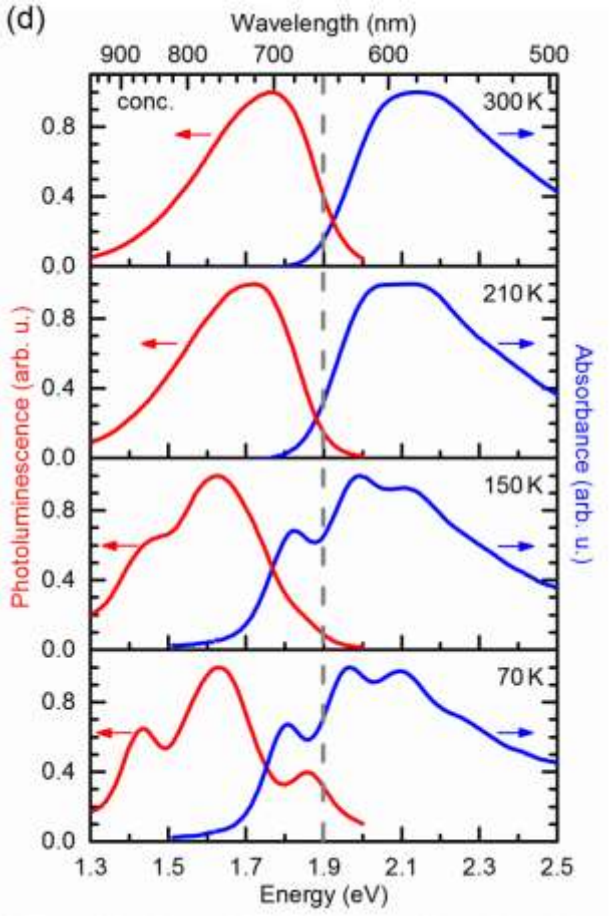
(d)
Wavelength (nm)
900 800 700 600 500
conc.
300 K
210 K
150 K
70 K
Photoluminescence (arb. u.)
Absorbance (arb. u.)
0.0 0.4 0.8
1.3 1.5 1.7 1.9 2.1 2.3 2.5
Energy (eV)

Figure 1: (a) Chemical structure of p-DTS(FBTTH$_2$)$_2$, along with photoluminescence and absorption spectra (b) taken in a $4.1 \cdot 10^{-5}$ M MTHF solution ("dil.") at four different temperatures (at 300 K, the emission taken in hexane solution is also indicated (dotted black line)), (c) taken from a thin film, spun-cast from a MTHF solution, at room temperature, and (d) taken in a $1.6 \cdot 10^{-4}$ M MTHF solution ("conc.") at four different temperatures. The vertical grey lines at 1.9 eV are a guide to the eye.

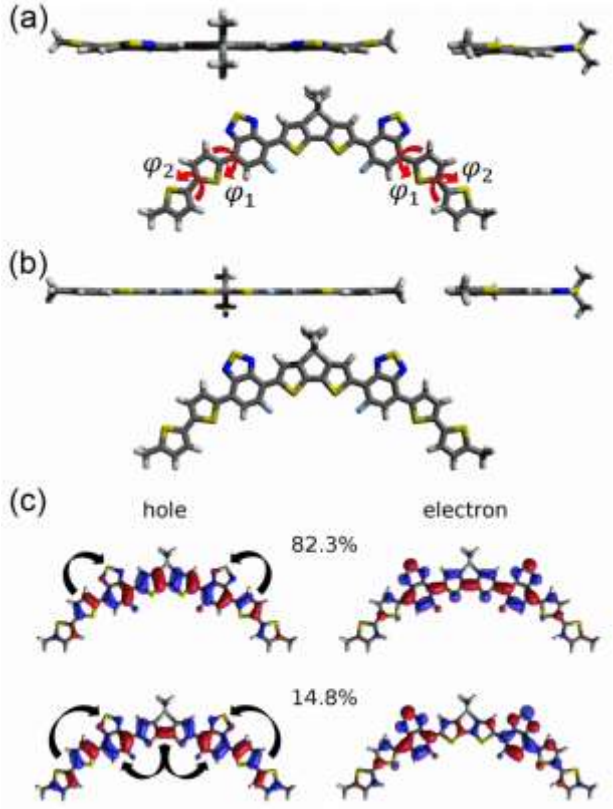

Figure 2: (a) Ground state geometry, with φ_1 = 11.9° and φ_2 = 17.5°, and (b) relaxed first excited state geometry, with φ_1 = 0.4° and φ_2 = 3.1°, of p-DTS(FBTTH$_2$)$_2$ in a THF solution, in side and top views, as obtained from quantum-chemical calculations. (c) Natural transition orbitals (NTOs) for the first singlet excited state of p-DTS(FBTTH$_2$)$_2$ in THF; hole orbitals depicted on the left, with corresponding electron orbitals on the right side of the figure. Values denote the contribution of a given pair of NTOs to the excitation. The arrows serve to highlight the changes in electron density.

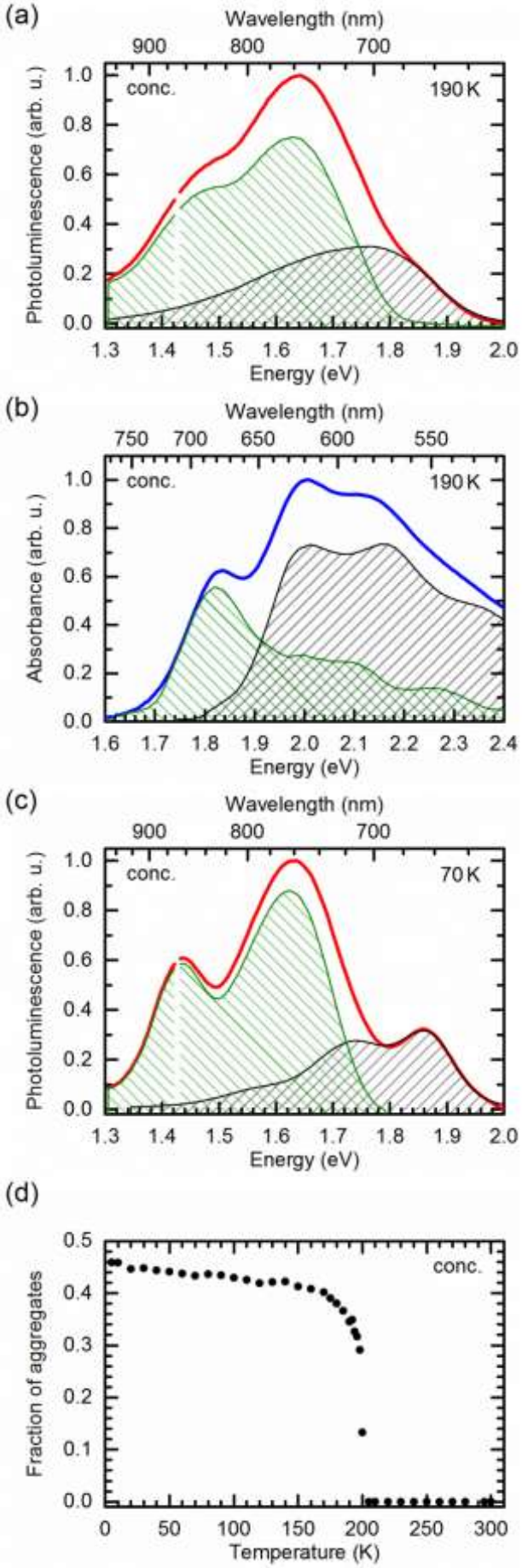
(a)
Wavelength (nm)
900
800
700
conc.
190 K
Photoluminescence (arb. u.)
Energy (eV)
(b)
Wavelength (nm)
750
700
650
600
550
conc.
190 K
Absorbance (arb. u.)
Energy (eV)
(c)
Wavelength (nm)
900
800
700
conc.
70 K
Photoluminescence (arb. u.)
Energy (eV)
(d)
conc.
Fraction of aggregates
Temperature (K)

Figure 3: Spectral deconvolution of (a) photoluminescence and (b) absorption spectra of p-DTS($FBTTH_2$)$_2$ (red and blue line) taken in a $1.6 \cdot 10^{-4}$ M MTHF solution at 190 K into a spectral contribution attributed to monomer (black filled line) and to aggregates (green filled line). Respectively, upon cooling (c) the photoluminescence spectrum at 70 K. (d) Fraction of aggregates of p-DTS($FBTTH_2$)$_2$ in a $1.6 \cdot 10^{-4}$ M MTHF solution as a function of temperature.

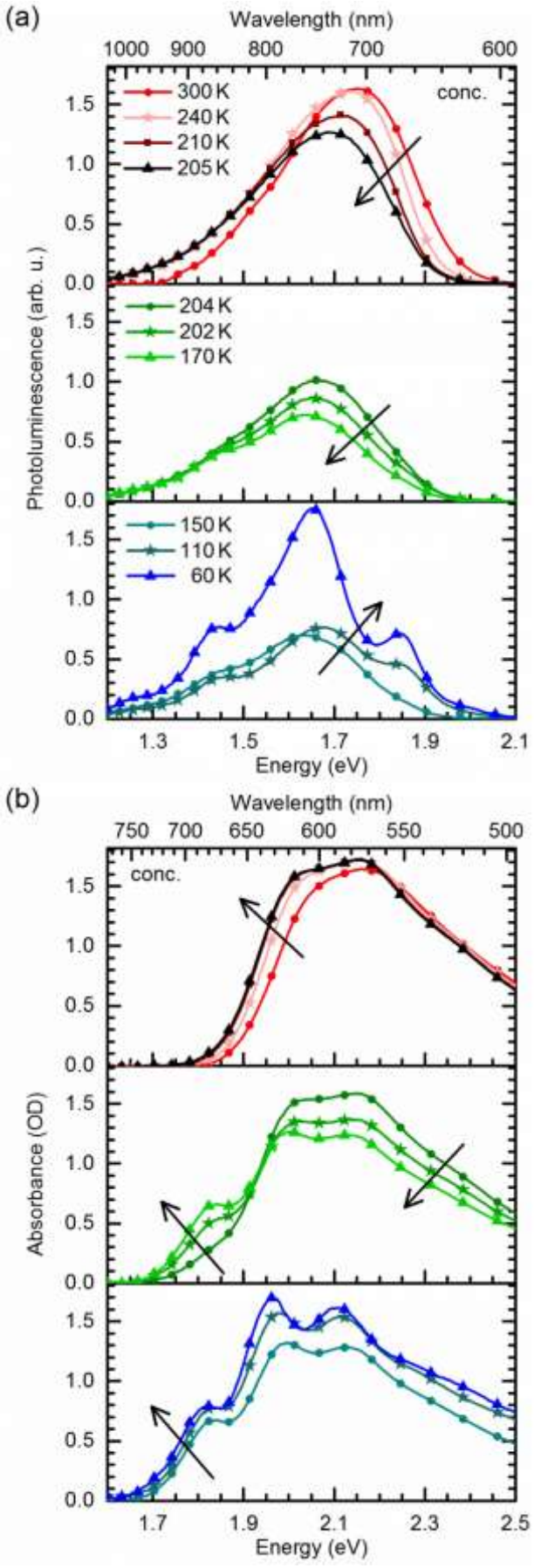
(a)
Wavelength (nm)
1000 900 800 700 600
300 K
240 K
210 K
205 K
conc.
204 K
202 K
170 K
150 K
110 K
60 K
Photoluminescence (arb. u.)
1.3 1.5 1.7 1.9 2.1
Energy (eV)
(b)
Wavelength (nm)
750 700 650 600 550 500
conc.
Absorbance (OD)
1.7 1.9 2.1 2.3 2.5
Energy (eV)

Figure 4: (a) Photoluminescence and (b) absorption spectra of p-DTS($FBTTH_2$)$_2$ taken in a $1.6 \cdot 10^{-4}$ M MTHF solution at different temperatures. The arrows indicate reducing temperature. For clarity of display, the spectra are separated into three distinct temperature ranges.

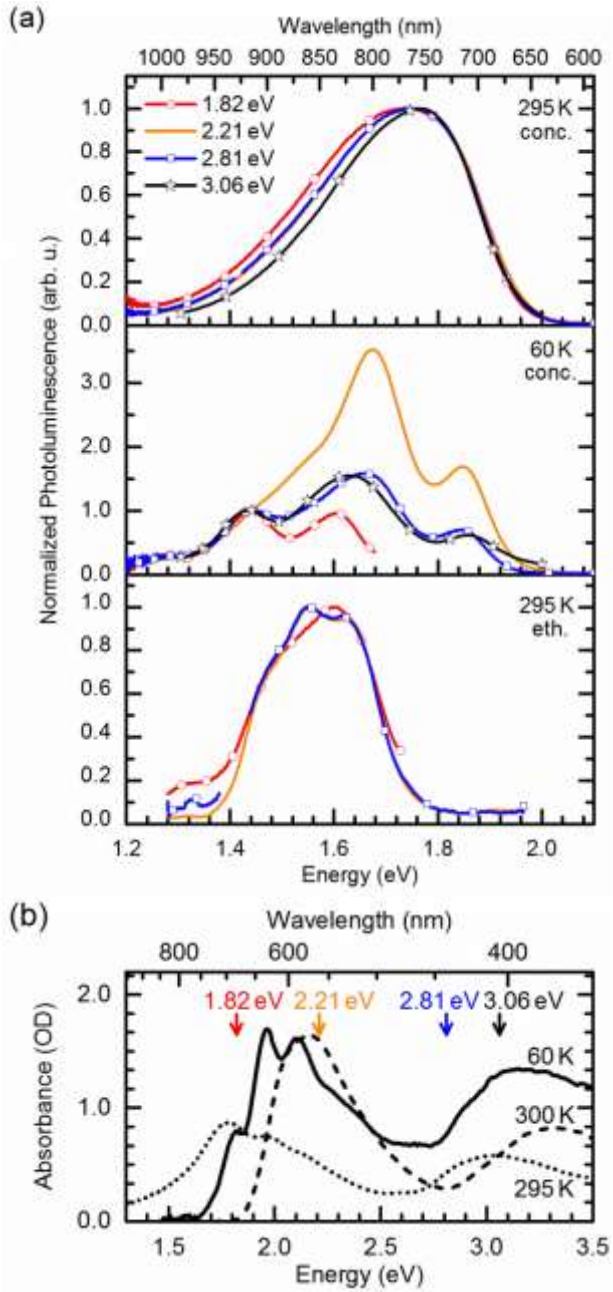

Figure 5: (a) Photoluminescence spectra of p-DTS(FBTTH$_2$)$_2$ for different excitation energies taken in a 1.6·10^{-4} M MTHF solution at 295 K (top), at 60 K (middle) and in a 1.0·10^{-4} M ethanol solution at 295 K (bottom panel). (b) Absorption spectra of p-DTS(FBTTH$_2$)$_2$ taken in a 1.6·10^{-4} M MTHF solution at 300 K (dashed line) and 60 K (solid line) and in a 1.0·10^{-4} M ethanol solution at 295 K (dotted line). The arrows are indicating the different excitation energies used for (a).

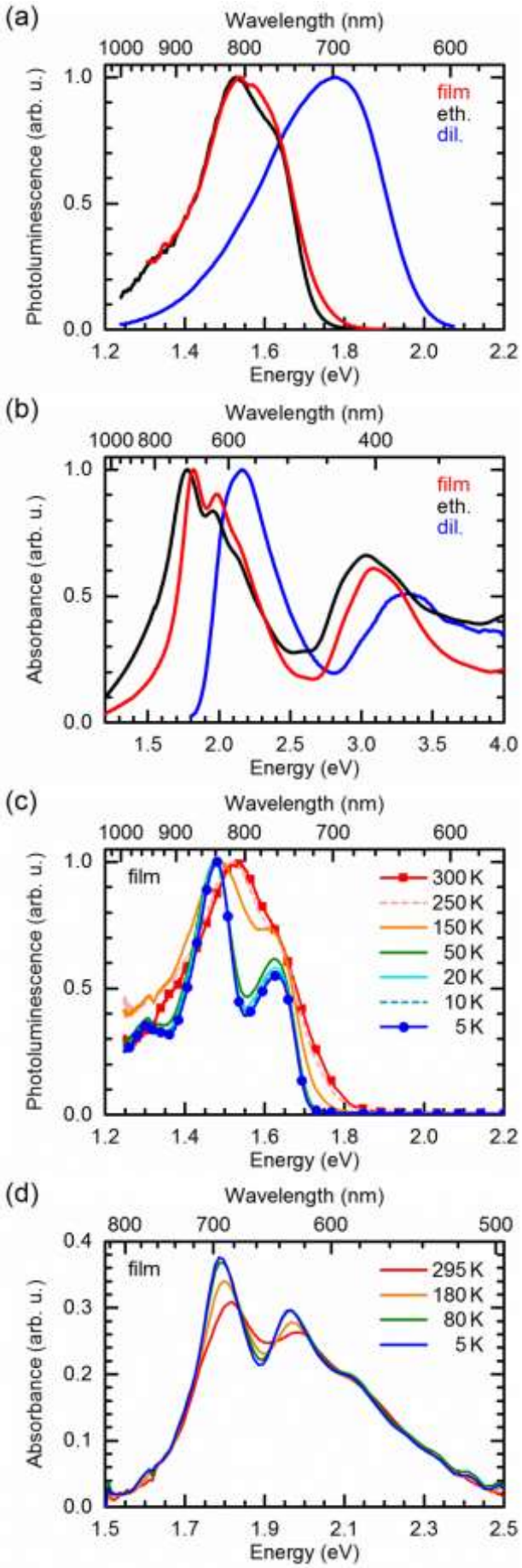
(a)
Wavelength (nm)
1000 900 800 700 600
Photoluminescence (arb. u.)
1.0
0.5
0.0
1.2 1.4 1.6 1.8 2.0 2.2
Energy (eV)
film
eth.
dil.
(b)
Wavelength (nm)
1000 800 600 400
Absorbance (arb. u.)
1.0
0.5
0.0
1.5 2.0 2.5 3.0 3.5 4.0
Energy (eV)
film
eth.
dil.
(c)
Wavelength (nm)
1000 900 800 700 600
Photoluminescence (arb. u.)
1.0
0.5
0.0
1.2 1.4 1.6 1.8 2.0 2.2
Energy (eV)
film
300 K
250 K
150 K
50 K
20 K
10 K
5 K
(d)
Wavelength (nm)
800 700 600 500
Absorbance (arb. u.)
0.4
0.3
0.2
0.1
0.0
1.5 1.7 1.9 2.1 2.3 2.5
Energy (eV)
film
295 K
180 K
80 K
5 K

Figure 6: (a) Photoluminescence and (b) absorption spectra of p-DTS($FBTTH_2$)$_2$ taken in a $4.1 \cdot 10^{-5}$ M MTHF solution (blue line), in a $1.0 \cdot 10^{-4}$ M ethanol solution (black line) and measured in a thin film (red line). (c) Photoluminescence and (d) absorption spectra of p-DTS($FBTTH_2$)$_2$ in a thin film at different temperatures.